3 Video Polarimetry

3.1 Simultaneous Video Polarimeters

The technique of video polarimetry developed by Prosch et al. (1983) generated the polarizational images of a scene instantaneously allowing real-time identification and selection of light sources of defined degrees and/or angles of polarization. Selected targets were scanned optoelectronically, and the digitised image information was stored by electronic means or could be displayed on-line. This was a measuring technique offering the advantages of instantaneous quick-look analysis, high-resolution wide field-of-view polarization maps in real time enabling the study of dynamic processes (e.g. motions or rippling water surfaces).

The video polarimeter of Prosch et al. (1983) consisted of three synchronously scanning imaging tubes (Plumbicon XQ 1270) equipped with linearly polarizing filters, spectral filters and lens systems. These three camera systems were mounted side by side on an optical bench carrying adjustment plates to align the optical axes (Fig. 3.1). The video signals were amplified, sampled and digitised. To generate false colour images in real time, a standard phase alternating line (PAL) composite video signal was generated. A minicomputer supported the system on-line transferring data from the AD-converters to magnetic tape, or processing the instantaneous radiances. Computational results were displayed simultaneously with the false colour image on the same screen. A colour ladder was generated and could be monitored atop the screen showing specific colours corresponding to predefined polarizational properties. A second display mode – colour representation of the voltage differences between the three channels – allowed to make sources of unpolarized light invisible on the screen. Three scan modes were available:

- In the manually controlled sampling, a cursor was positioned within the screen, the related video signals were continuously digitised and processed, and the degree and angle of linear polarization as well as the components of the Stokes vector were displayed on the same screen.
- The repetitive one-dimensional horizontal scan was used in case of air-borne measurements, when the instrument was operating as a cross-track scanner.
- Using the two-dimensional scan of the complete field of view, stationary imaging was performed, where all sampled and digitised data were transferred

directly to magnetic tape. The final data evaluation was done off-line by a powerful computer.

In the calibration of their instrument, Prosch et al. (1983) took into account the measured incident-angle-dependent response of the imaging tubes across the field of view, and the analytically calculated incident-angle-dependent dichroic extinction properties of the polarizing filters. After calibration, the video polarimeter could measure the degree of linear polarization p by an error less than 3%. The error $\Delta\alpha$ in determination of the angle of polarization α depended strongly on p and on the radiometric precision r of the imaging tubes. The smaller the value of p and/or r, the larger was $\Delta\alpha$.

In this video polarimeter, three voltages were generated, which were proportional to the radiances. Coding a colour TV signal by these voltages, the resulting colour vector was determined for a standard PAL composite video signal. Using the resulting normalized colour vector in a standard two-dimensional colour table with p as parameter, the Stokes vector was projected in the colour table in such a way, that unpolarized light was white, and increasing p caused a deviation from these colourless loci. α defined the tint, whereas p was represented by the hue. Prosch et al. (1983) used 60^o spacing between the orientation of the transmission axes of the polarizers, because then the discernability of the colour-coded polarization status was improved in comparison with that for a 45^o spacing, which is commonly used in other polarimeters.

The pioneering video polarimeter of Prosch et al. (1983) has been flown in an aircraft over different terrain features and lakes. Over land, many features have been made much more clearly discernible than with unpolarized radiance measurements only. Prosch et al. (1983) suggested, that p is a useful source of information for remote earth resource observations.

Hanlon et al. (1999) designed a simultaneous video polarimeter based on a standard three-tube camera using a dichroic prism block for colour separation. This prism is replaced with a neutral prismatic beam-splitter such that each of the three videochannels receive one third of the broad-spectrum image input. Since this assembly lacks the colour-trimming filters cemented to the original dichroic prism, magnification errors due to pathlength differences are corrected with small quartz discs of appropriate thickness. A small disc of linear polarizer (HNP'B, Polaroid) is placed immediately in front of each camera tube to impart polarization sensitivity to the channels. The direction of the transmission axis of the polarizers is 0^o, 45^o and 90^o from the vertical. The camera electronics encodes the three polarizational images as if they were colour, making it possible to store all the data on a regular portable videocassette recorder and allowing for immediate viewing of a colour-coded polarization pattern on a colour monitor in such a way that unpolarized regions of the scene are colorless, whereas polarized areas appear false-coloured. The signal in all three channels is identical, and the output of the tubes is adjusted to give white for overexposure. Monochromatic images of a scene taken from the three channels separately can be transferred through a frame grabber into a computer and their degree and angle of linear polarization can be

calculated. This simultaneous video polarimeter was used for aerial recording of the polarization patterns of cephalopods moving in an aquarium.

3.2 Sequential Imaging Polarimeters Using Liquid Crystal Polarizers

Obtaining the polarizational pictures by rotating a polarizing filter in front of an intensity detector is a mechanically active process that may produce optical distortion if the plane of the filter is not exactly perpendicular to the optical axis of the camera and is difficult to fully automate. Using liquid crystals (LCs), errors caused by mechanical rotation (e.g. inertia with acceleration and brake times, misalignments of the signal on the detector) can be eliminated. The main disadvantage is that the retardation introduced by a LC is dependent on external factors, such as the temperature, for example.

Twisted nematic LCs have a helical molecular structure, which gradually rotates from one side of the crystal to the other; the degree of rotation is preset during the manufacture (Priestly et al. 1975). The molecules can be stretched by applying an alternating voltage; when the voltage is zero, the molecules return to their twisted stage. The angle of polarization α of partially linearly polarized light transmitted through the LC is rotated by a preset value. When the molecules of the crystal are stretched, α of the transmitted light is not changed. These LCs do not distort the geometry of the incoming image, and transmit light across a broad band of the spectrum. However, time (several 10 ms) is required for stretching and relaxing the molecules.

Wolff (1993) designed an imaging polarimeter using a monochrome CCD camera with a fixed linearly polarizing filter and two twisted nematic LCs set between UV-absorbing glass plates in front of the lens system of the camera. The LCs can rotate electro-optically the totally polarized component of the incoming light by a given angle φ, while they do not affect the unpolarized component. Wolff (1993) used $\varphi = 0^o$, 45^o and 90^o to take three polarizational pictures from a given scene. Hence, in this case not the linearly polarizing filter rotates mechanically at a fixed α of the incident light, but the filter is fixed and α is rotated electro-optically prior to the transmission through the filter. The results are the same as if the filter was rotated. A driver for the LCs modulates a high frequency alternating voltage so as to produce the mentioned three rotational (or twist) states of the two LCs. The driver also provides synchronization, which ensures that an image from the camera is digitised when the LC is in a fully relaxed state, and ensures that the twist state of both LCs is known with respect to each digitised image.

After computer evaluation of the three polarizational images, a false-coloured picture is obtained, which displays the distribution of intensity, degree and angle of linear polarization in the composite (hue-saturation-brightness) visualization scheme. Using a colour video camera for recording polarizational images that are analysed at a later stage, Cronin et al. (1994) and Shashar et al. (1995a,b) built a

portable version of the sequential imaging polarimeter of Wolff (1993). The state of the LCs is independently recorded by placing small linearly polarizing stripes in the field of view of the camera. In the laboratory, an on-line version of the polarimeter is used based on a digital camera connected to a personal computer. The electronic card controlling the twist and relaxation of the LCs is synchronized with the video signal of the camera. Both polarimeters can be placed in waterproof protective submersible housings for underwater measurements. Cronin et al. (1994) and Shashar et al. (1995a,b) used their portable and submersible polarimeter to record polarization patterns occurring in a tropical rain forest and in submarine habitats (e.g. coral reefs, underwater objects and animals).

3.3 Mueller Matrix Sequential Imaging Polarimeter

Pezzaniti and Chipman (1995) has built the first Mueller matrix imaging polarimeter. Mueller matrix polarimeters are widely used to measure different polarizational properties in optical systems and samples. Most of these systems are point-source polarimeters.

Using a CCD camera as detector in the recording state and liquid crystals (LCs) adapted to an ophthalmoscopic double-pass apparatus, Bueno and Artal (1999) designed a Mueller matrix imaging polarimeter in order to calculate spatially resolved Mueller matrices of the human eye. The theoretical basis of this system is described by Bueno (2000a). The polarimeter uses a pair of LC variable retarders (LCVRs), both in the input and output optical paths. A LCVR is composed of a fixed linearly polarizing filter followed by a LC cell, which can rotate the E-vector of linearly polarized incident light, and thus can produce three independent polarizational states. The first LCVR acts as a polarizational state generator (PSG) and the second as a polarizational state analyser (PSA). In transmission mode, the sample is placed between the two LCVRs, between the PSG and PSA. For a fixed position of the generator-analyser system, only $3\times3=9$ elements of the Mueller matrix can be obtained, because 9 independent polarizational states can be generated by the two LCVRs. A removable quarter-wave plate (RQWP) can produce the fourth independent polarizational state. The effect of such a plate is to rotate counter-clockwise the incident Stokes vector at an angle of 90^o around its fast axis. Thus, the other 7 elements of the Mueller matrix are accessible when two RQWPs, one behind the PSG and other in front of the PSA, are introduced. In this way, $4\times4=16$ intensities are recorded, each corresponding to a different independent[1] combination of polarizational states of the PSG-PSA system. The calculation of the Mueller matrix (completely describing the polarizational properties of the sample) involves 16 independent images, that is, 16 independent linear equations of intensity measurements at every pixel. This system of

[1] In mathematical terms, 4 vectors with 4 components are independent, if the determinant of the 4×4 matrix composed by them is not zero. For Stokes vectors, the largest possible value of this determinant is 2, meaning total independence.

equations can be solved by a matrix inversion method, for example. This Mueller matrix imaging polarimeter allows to obtain the polarizational properties of static samples both in transmission and reflection mode. It can be used, for instance, in the study of polarizational characteristics of substrata and samples with anisotropic layers, scattering effects at rough surfaces and *in vitro* samples (e.g. Bueno 2000b, 2001; Bueno and Artal 1999, 2001; Bueno and Jaronski 2001).

3.4 Sequential Imaging Polarimeter Using Beamsplitter and Liquid Crystal Polarizer

To speed up the time of measurement, Wolff (1994) as well as Wolff and Andreou (1995) used a polarizing plate beamsplitter to direct light onto two CCD detectors and a twisted nematic liquid crystal in front of the beamsplitter to rotate the angle of polarization of the transmitted light. With this instrument two sequential recordings with two polarizational image pairs is needed instead of three. After evaluation, the intensity, degree and angle of linear polarization are obtained with pixel resolution and visualized in the hue-saturation-brightness scheme. This instrument is not portable and can function only in the laboratory at its present state of development.

3.5 Rotating-Analyzer Sequential Video Polarimeter

Horváth and Varjú (1997) used a rotating-analyser sequential video polarimeter to measure the polarization patterns of different terrestrial objects and habitats. Their aim was to obtain a database, a "digital atlas of polarization patterns". The four main steps of their technique, based on a video camera set up on a tripod are illustrated in Fig. 3.2. A given scene is recorded by a video camera through a neutral density rotatable linearly polarizing filter in front of the objective lens. Prior to recording, the focus, aperture, shutter speed and gain are manually selected. The initial alignment of the transmission axis of the polarizer is vertical. After a few seconds, it is turned manually twice by 45^{o} counter-clockwise. The actual direction of the transmission axis is spoken into the built-in microphone during recording.

The recorded scenes are digitised frame-by-frame using a frame grabber in the computer connected to a video recorder. The digitised response of the single pixels of the CCD detector is approximately a linear function of brightness when light intensities are not too high. In order to remain in this linear region, an appropriate set of values of the aperture, shutter speed and gain must always be selected, a procedure that requires a high level of experience. For all three orientations of the polarizer´s transmission axis 25 digitised frames can be averaged to filter the inevitable small noise of the video signal. After calibration of the camera/frame grabber combination for response versus intensity coding, from

these three averaged colour video pictures, the modulation of the intensity I is obtained as a function of φ. A sinusoid $I = A\ sin2(\varphi - \alpha + \pi/4) + B$ is fitted to this intensity modulation for each pixel of the picture in order to determine $I_{max} = B + A$, $I_{min} = B - A$ and the angle of polarization α, that is, the angular position of I_{max}. From these parameters the total intensity $I = (I_{max} + I_{min})/2 = B$ and the degree of linear polarization $p = (I_{max} - I_{min})/(I_{max} + I_{min}) = A/B$ are calculated for every point in the image.

Finally, two-dimensional colour- or grey-coded maps of I, p and α are produced with pixel resolution in the red (650 nm), green (550 nm) and blue (450 nm) spectral ranges, in which the three colour-sensitive CCDs of the camera have their maximal sensitivity. The outputs of this technique are 3×3 pictures of the scene recorded: the two-dimensional patterns of the intensity, degree and angle of linear polarization measured in the red, green and blue spectral ranges (Fig. 3.3).

3.6 Sequential Stereo Video Polarimetry: Visualizing Polarization Patterns in Three Dimensions

Mizera et al. (2001) realized stereo video polarimetry, by which polarization patterns can be visualized in three dimensions. This method is applicable to both scientific and educational purposes despite that there is no information that any animal visual system uses polarization as an input of binocular fusion, or stereopsis. The essence of stereo video polarimetry is the addition of depth to scenes imaging the distribution of polarization. Stereo video polarimetry is actually nothing more than the match-making of two different methods, namely, stereoscopic imagery (e.g. Brown 1994; Drouin 1995) and imaging polarimetry.

During a stereo video-polarimetric recording two video-polarimetric recordings of the investigated scene must be performed from two different, properly selected directions of view (Fig. 3.2A) to simulate the distance between the two eyes. Mizera et al. (2001) moved the camera by about 6 cm between the two images, which baseline corresponds with the average distance between the two human eyes but exceeds the ocular separation in several animals having polarization sensitivity.

In order to obtain a stereo effect of high quality one has to follow the general guidelines of stereo imagery (e.g. Waack 1985; Burder and Whitehouse 1992). The most common viewing method of stereo pairs is known as parallel, or free, or wall-eye viewing, and is reached most conveniently with the help of proper stereoscopic viewing lenses or prisms (Fig. 3.2E). Without such devices, one can use simply the palm of the hand or a sheet of paper (Burder and Whitehouse 1992). The palm of the hand or the sheet must be held vertically in front of the nose, parallel to the symmetry plane of the head. By selecting properly the distance of the eyes from the stereo pair, one can arrange that the left eye looks at, and only at, the left image, and the right eye looks at the right image (Fig. 3.2E), then in the mind a three-dimensional image is formed.

As an example, Fig. 3.4 shows the stereo pairs of the reflection-polarization patterns of a car with a shiny bodywork measured with stereo video polarimetry. We can see in rows 2 and 3 of Fig. 3.4 that in some regions of the scene, p and α change strongly from point to point, which results in a rather erratic false colour distribution in these regions. The consequence of this is that the false colours of a given pixel on the stereo pair can be frequently different. Thus, the three-dimensional image cannot be developed, or at least the stereo effect is considerably reduced, because the mind of the observer is not able to or can hardly discover the corresponding pixels in the stereo pair.

The human visual system extracts spatial information from the two, slightly different images perceived by the right and left eyes on the basis of retinal disparities. Our mind is not adapted to reconstruct three-dimensional (3D) images from false-coloured stereo pairs encoding the spatial distribution of polarization. This is the reason why the 3D image is so difficultly formed when viewing the fully false-coloured stereo pairs of p and α. Thus, our mind needs some help to produce the 3D image of a polarized scene. Such help can be the use of the false colour combination of the stereo pair of the colour picture and the polarization patterns of the investigated scene.

Rows 4 and 5 in Fig. 3.4 show the stereo combination of the intensity (I) distribution of the car with the p- and α-pattern, respectively. In these combined stereo pairs I is coded by the brightness and the polarization information is displayed by the colour. The function of the stereo pair of the I-pattern of the scene in a given spectral range (rows 4 and 5 of Fig. 3.4) is to construct a "visual skeleton", on the basis of which the 3D image can be formed. This skeleton is then filled with the polarization information, either p or α, which is coded by colour shades.

Until now there is no evidence of binocular polarization channels in any visual system, just as there is no combination of colour binocularly in animal or human vision (stereo vision is achromatic and polarization-blind). Thus for this reason stereo video polarimetry is nothing else as a useful technique to visualize for a human observer how polarization varies with distance in a scene.

3.7 Ultraviolet-Sensitive Rotating-Analyzer Sequential Video Polarimeter

Horváth and Wehner (1999) designed a portable, UV-sensitive rotating-analyser sequential video polarimeter, which is composed of a tube camera (Hamamatsu Beam Finder III) with spectral sensitivity ranging from 200 to 750 nm. In front of the objective lens system a rotating linearly polarizing filter (HNP'B, Polaroid) is mounted with good polarizational characteristics also in the UV-C range of the spectrum (300 nm $< \lambda <$ 400 nm). Onto this polarizer a colour filter can be screwed on. If this is an UV-transmissing filter, video-polarimetric measurements can be performed in the UV. Using colour filters with transmission maxima in the

visible spectral range, the polarization patterns can be measured in the visible part of the spectrum.

The camera set on a tripod is connected to a portable video recorder (Sony 8 mm video walkman GV-S50E) for data storage. All technical details are spoken into a microphone and recorded as an audio signal by this video walkman too. The recording, evaluation and visualization of the polarization patterns happen similarly as in the case of the normal video polarimetry described above. To obtain light intensity data that are proportional to the real radiant intensities in a given range of the spectrum, the spectral transmission characteristics of the polarization filter and the camera optics as well as the spectral sensitivity of the camera sensor are taken into account. With this UV-sensitive video polarimeter the polarization patterns of the sky (Horváth and Wehner 1999) and the reflection-polarizational characteristics of water surfaces (Bernáth et al. 2002) were studied both in the UV and visible parts of the spectrum.

3.8 Sequential Video Polarimeters using Microscopes

3.8.1 Polarization Video Microscopy

Shashar et al. (2001) equipped a Zeiss SVII dissecting microscope with a digital camera and a rotatable linearly polarizing filter (HN38S) installed in the outgoing light path. Taking three consecutive images through the polarizer at three different directions of its transmission axis under depolarized epi-illumination, the p- and α-patterns of the target in the microscope can be determined as in the case of other types of imaging polarimetry.

3.8.2 Differential Polarization Laser Scanning Microscopy

In differential polarization (DP) microscopy the images are constructed from data derived from measurements using two orthogonally polarized light beams in the excitation or emission and light scattering pathway. The resulting images are two-dimensional maps of the measured DP and carry information on the anisotropic structure of the microscopic sample and/or the interaction of the sample with polarized light. In contrast to the macroscopic DP (usually representing a mean value after averaging for the whole sample volume) microscopic DP directly relates to a well-defined and oriented microscopic volume of the sample. Thus microscopic DP maps local DP properties in the sample within the constrains of the resolution of light microscopy.

Polarized light microscopy (e.g. Módis 1991; Robinson and Bradbury 1992) usually provides qualitative information, and is limited to some relatively easily determinable quantities, such as linear birefringence and linear dichroism, for

example. It is also used to enhance the contrast of the microscopy images. The performance of classical polarization microscopy can be improved considerably by applying digital recording and image analysis (e.g. Kocsis et al. 1998). Passive polarizers have been utilized in laser scanning microscopy (LSM)[2] either in the transmitted or in the fluorescence beam (Verbelen and Kerstens 2000). This technique can reveal the presence of certain anisotropic structures in the sample.

In DP microscopy usually well-established techniques of DP spectroscopy are employed: (i) high frequency modulation produces two orthogonally polarized states of light for the excitation; or (ii) the emitted or scattered light is analyzed for its content of orthogonally polarized components. Data in each pixel are obtained after demodulation and calculation of the DP quantities. DP microscopy provides much better resolution and higher sensitivity than the conventional polarization microscopy.

For transmitted and scattered light, theory of DP imaging has been elaborated by Kim et al. (1987). 16 independent Mueller DP images can be obtained which all carry information on specific light-matter interactions. Some of these images, such as patterns of the linear dichroism (LD) or circular dichroism (CD) are of special importance, and have been measured by using an image dissector camera (Beach et al. 1987) and a scanning confocal-stage microscope (Finzi et al. 1989). In a polarization modulation laser scanning microscope (Gupta and Kornfield 1994) DP imaging has been used in the transmission regime of a laser scanning microscope to determine LD and linear birefringence of polymer films with high sensitivity and precision.

Recently, a differential polarization laser scanning microscope (DPLSM) has been constructed by Pomozi (2002), Garab et al. (2003) and Pomozi et al. (2003). This technique is based on a Zeiss LSM 410 and uses high frequency modulation techniques. It can measure the following quantities:

- Fluorescence emission anisotropy r, which reflects the linear polarization of the luminescence emission and provides information on the anisotropic distribution of the emission dipoles.
- Circularly polarized luminescence (*CPL*) content of the emission, providing information on the chiral structure of the sample.
- The degree of linear polarization (p) of the fluorescence emission upon an excitation of the sample with linearly polarized light, allowing conclusion e.g. on energy transfer between the dipoles, the microviscosity of the sample in the vicinity of the emitting chromophore, and its excitation lifetime.

[2] In LSM the objective lens focuses a laser beam to a well-defined volume of the object at the focal point. By raster scanning a rectangular field, the intensity distribution of reflected or emitted light originating from the illuminated points is determined and stored as a digital image of the scanned area. Positioning a pin-hole in front of the detector in the fluorescence beam, only the light from the irradiated volume passes through to the detector and the light originating from out of the focal plane is filtered. The confocality provides optical slicing of the sample and clearer pictures.

- Linear dichroism (*LD*), providing information on the anisotropic distribution of the absorbance dipoles.
- Circular dichroism (*CD*) signals, being given rise by chirally organized molecules and/or molecular assemblies.
- Fluorescence-detected linear and circular dichroisms (*FDLD* and *FDCD*), providing the same information as *LD* and *CD* but with the use of fluorescence detection and thus reducing the effect of scattering.

Linear and circular birefringence patterns are given rise in anisotropic and optically active materials. For all DP parameters which use fluorescence, i.e. *r*, *p*, *FDLD* and *FDCD*, the images can be recorded in confocal regime, which thus provides better spatial resoltuion and the possibility of optical slicing and three-dimensional reconstruction.

Figure 3.5 shows the DP patterns of a phloem of *Convallaria majalis* measured by differential polarization laser scanning microscopy. Figure 3.5A shows the pattern of the fluorescence intensity *I* upon unpolarized excitation. Figures 3.5B and 3.5C display the patterns of anisotropies r_0 (with respect to the horizontal) and r_{45} (relative to 45º from the horizontal). The fluorescence anisotropy *r* is the ratio of the difference between the intensities of the two orthogonally polarized components of emitted light upon the unpolarized excitation and the total intensity of emission. The bright and dark areas indicate positive and negative *r*-values, respectively. The white parts of the *r*-images represent very low intensities *I*, where the determination of *r* is ambigous. Figures 3.5B,C show that *r* depends significantly on the orientation of different parts of the cell wall. Figure 3.5D displays the change of *I*, r_0 and r_{45} along the black line in Figs 3.5A-C. It is clear from Fig. 3.5D that the variations in *r* are not correlated with those in *I*, but identify the orientation of fibers in the cell wall.

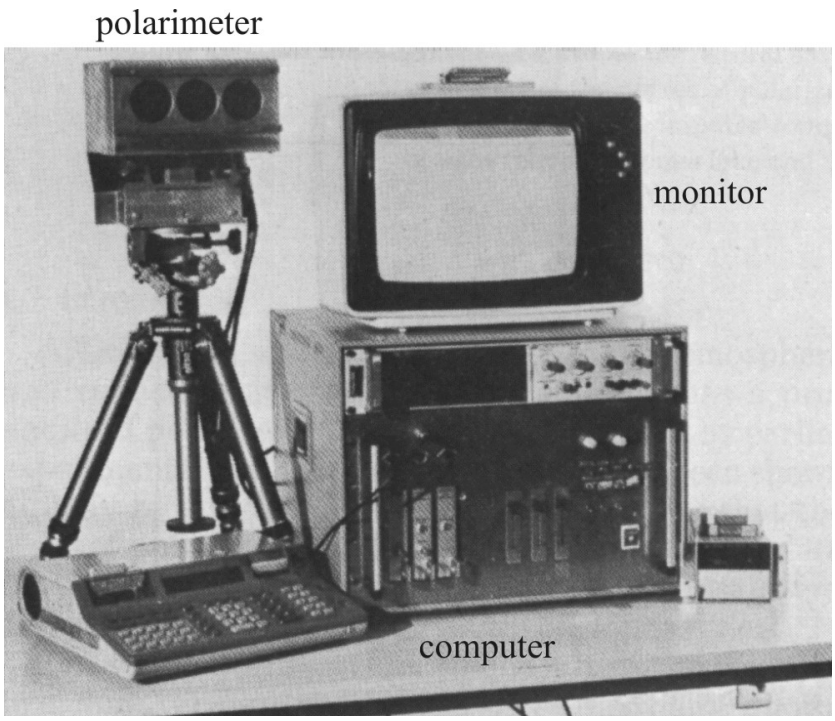

Fig. 3.1. The video polarimeter designed by Prosch et al. (1983, Fig. 4, p. 1362).

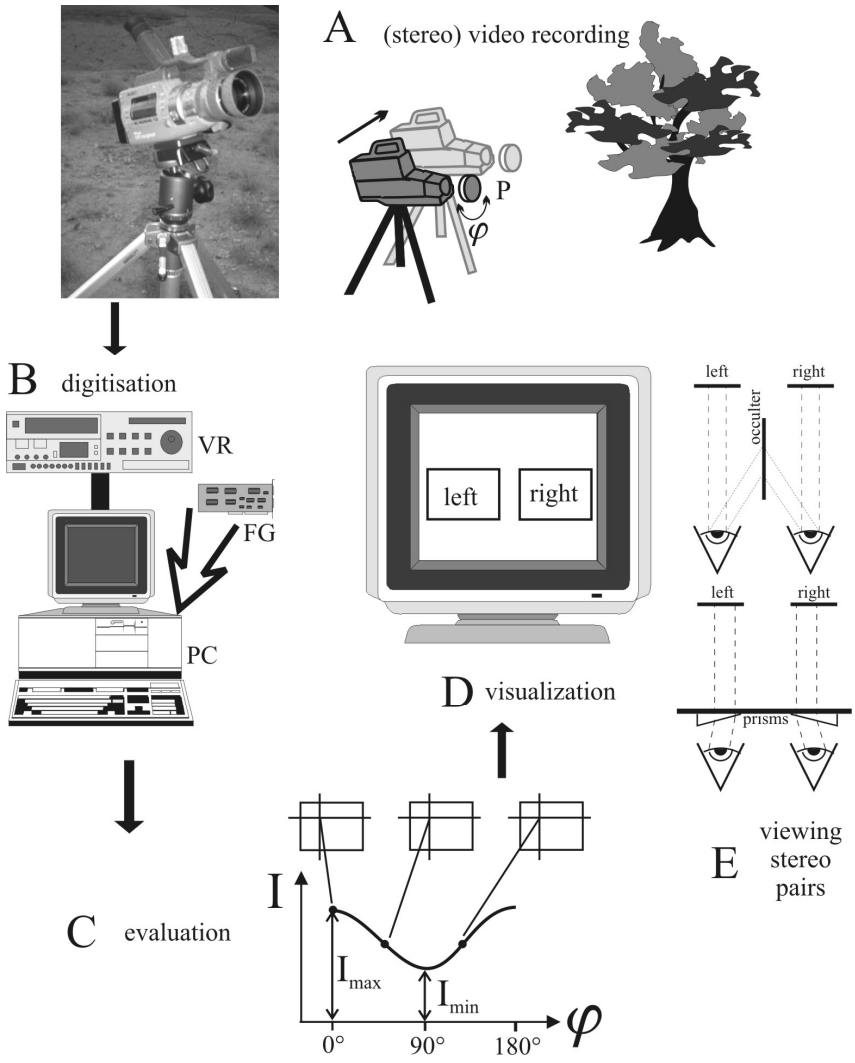

Fig. 3.2. Schematic representation of the technique of rotating-analyzer (stereo) video polarimetry. A: Recording with a video camera mounted with a rotating linearly polarizing filter (P) in front of the objective lens. At stereo video polarimetry two recordings are taken from two different directions of view. φ: angle of rotation of the transmission axis of the polarizer. B: Digitisation of the recorded pictures using a frame grabber (FG) in a personal computer (PC) connected directly to the video camera recorder or to a video recorder (VR). C: Evaluation of the light intensity I, the degree of linear polarization p and the angle of polarization α from pixel to pixel of the recorded scene. D: Visualization of the patterns of I, p and α on the computer screen (in the case of stereo video polarimetry in form of false coloured stereo image pairs). E: Two common possibilities of viewing stereo pairs with the use of an occulter or prisms. (After Fig. 1 of Mizera et al. 2001, p. 395).

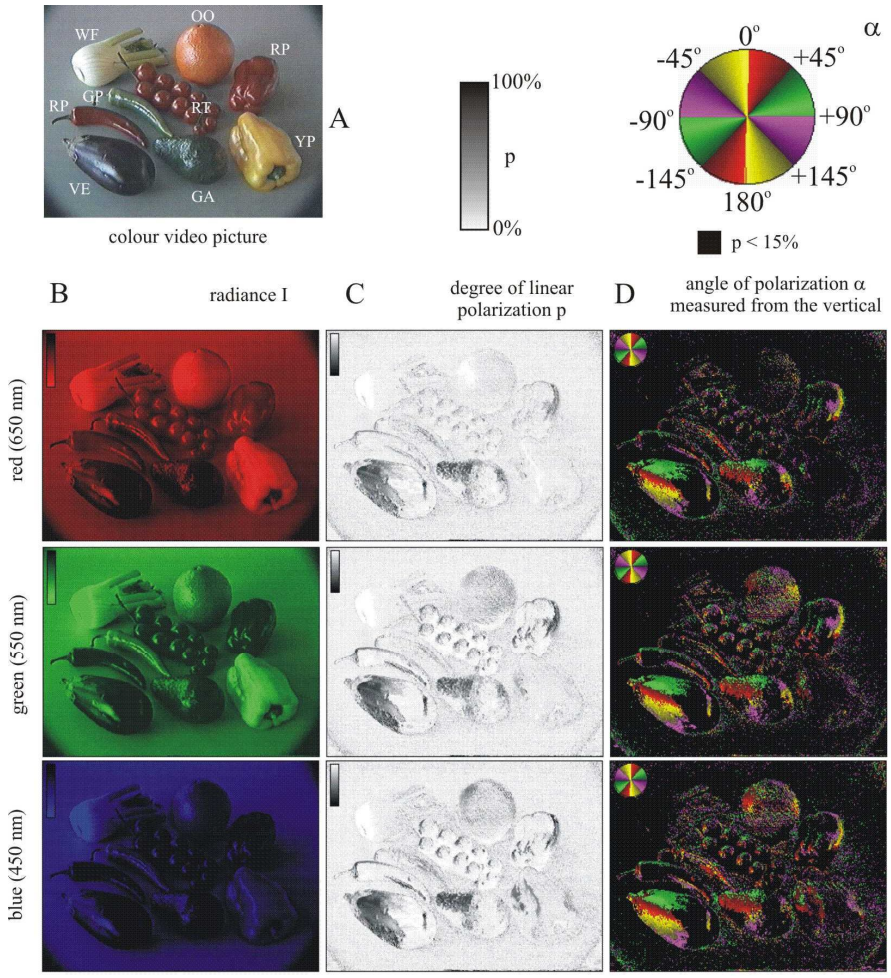

Fig. 3.3. A: Video picture of a collection of fruits and vegetables of different colours. B-D: The patterns of the intensity I, degree of linear polarization p and angle of polarization α of light reflected from the collection measured by video polarimetry in the red (650 nm), green (550 nm) and blue (450 nm) ranges of the spectrum. The different numerical values of I, p and α are coded by different colour and grey tones as shown in the insets. In the α-patterns black represents areas with $p < 15\%$. WF: white fennel root, OO: ochre orange, RT: red tomato, RP: red paprika and red pepper, YP: yellow paprika, GP: green pepper, GA: green avocado, VE: violet egg-fruit. (After Fig. 2 of Horváth and Varjú 1997, p. 1157).

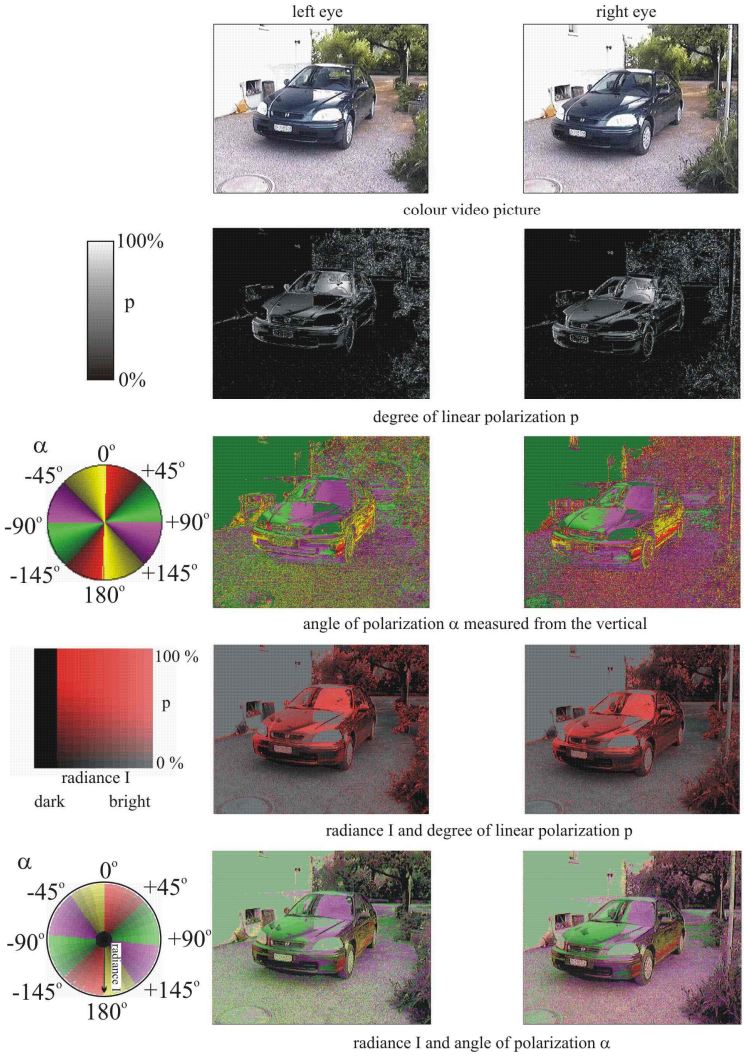

Fig. 3.4. The reflection-polarizational characteristics of a car with a shiny bodywork represented in parallel view stereo format and the corresponding colour and grey palettes encoding the numerical values of the degree of linear polarization p and angle of polarization α. First row: Stereo pair of the colour video picture of the car. Second row: Stereo pair of the p-pattern measured in the green (550 nm). Third row: Stereo pair of the α-pattern at 550 nm. Fourth row: Stereo pair of the combined patterns of p and radiance I. The higher the p-value, the deeper is the red hue. If $I < 20\ \% = I_{threshold}$, then p is not represented by red. We used $I_{threshold}$, else due to the inevitable small noise of p at low I-values erratic deep red patches or pixels would be occur in the picture. Fifth row: Stereo pair of the combined patterns of I and α. The higher the I-value, the brighter the colours coding α. The same $I_{threshold}$ is used again as in row 4 to remove the noise of α at low I-values.

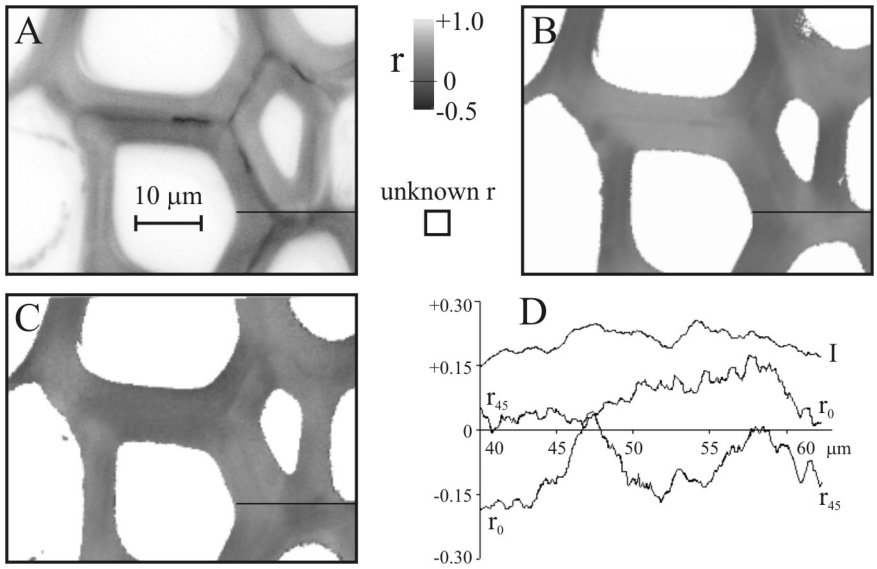

Fig. 3.5. Patterns of the fluorescence intensity I (A), anisotropy r_0 relative to the horizontal (B) and anisotropy r_{45} relative to 45º from the horizontal (C) measured by differential polarization laser scanning microscopy. D: Quantitative data of I, r_0 and r_{45} measured along the black line in A-C. I is displayed on an arbitrary scale in such a way that darker grey shades code higher I-values. (Courtesy of G. Garab and I. Pomozi, Biological Research Center, Hungarian Acadmey of Sciences, Szeged).